Contact-Free Measurement of Cardiac Pulse Based on the Analysis of Thermal Imagery

Marc Garbey, Nanfei Sun, Arcangelo Merla, and Ioannis Pavlidis*, *Senior Member, IEEE*

***Abstract*—We have developed a novel method to measure human cardiac pulse at a distance. It is based on the information contained in the thermal signal emitted from major superficial vessels. This signal is acquired through a highly sensitive thermal imaging system. Temperature on the vessel is modulated by pulsative blood flow. To compute the frequency of modulation (pulse), we extract a line-based region along the vessel. Then, we apply fast Fourier transform (FFT) to individual points along this line of interest to capitalize on the pulse's thermal propagation effect. Finally, we use an adaptive estimation function on the average FFT outcome to quantify the pulse. We have carried out experiments on a data set of 34 subjects and compared the pulse computed from our thermal signal analysis method to concomitant ground-truth measurements obtained through a standard contact sensor (piezo-electric transducer). The performance of the new method ranges from 88.52% to 90.33% depending on the clarity of the vessel's thermal imprint. To the best of our knowledge, it is the first time that cardiac pulse has been measured several feet away from a subject with passive means.**

***Index Terms*—Adaptive filtering, cardiac pulse, fast Fourier transform (FFT), medical imaging, thermal imaging.**

I. Introduction

CARDIAC pulse monitoring is widely used in health care, sport training, sleep studies, and psycho-physiological examinations. Various contact measurement methods have been developed to estimate a subject's cardiac pulse. These measurement methods capitalize upon the electrophysiological and mechanical processes associated to the heart activity and blood circulation. The golden standard for pulse measurement is Electro-Cardio-Graphy (ECG) [1]. ECG records the electric potential generated in different parts of the body due to the propagation of the action potential in the cardiac muscular fibers. ECG recording requires the use of a signal bio-amplifier and at least three contact electrodes coupled to the skin through a conductive gel.

Other pulse measurement devices can be used when one is interested mainly in the cardiac frequency and the shape of the cardiac signal in the peripheral circulatory system. Such devices quantify the pulse through indirect mechanical effects of blood flow or arterial pressure change in the vascular network of a tissue. A popular device that belongs to this category is the piezoelectric transducer. It is attached to the finger of a subject and converts local blood pressure variations, associated with cardiac activity, to a voltage signal [2]. This is a reliable measurement method, but it is sensitive to motion. We use a piezoelectric device as the ground-truth (GT) standard of comparison against our thermal imaging (TI) analysis method [3].

Doppler ultrasound is a more advanced technology that is used to collect blood velocity spectra. Holdsworth *et al.* first recovered the full pulse waveform of the carotid based on blood velocity spectra in 1999 [4]. Ultrasound measurements still require contact between the probe and the subject, as well as the use of a special gel to facilitate wave transmission.

Photoplethysmography (PPG) is another pulse measurement method that capitalizes upon the optical properties of a selected skin area. For this purpose near-infrared light is emitted into the skin. More or less light is absorbed, depending on the blood volume in the skin. Consequently, the backscattered light corresponds to the variation of the blood volume associated to the cardiac pulse. PPG is used widely to measure the pulse waveform [5], pulse wave reflection [6], dermal perfusion [7], and microcirculation [8]

Laser Doppler sensing can also measure cardiovascular pulse by quantifying the minute skin displacement caused by the pressure wave propagation [9]. Initially, the need for large and expensive Michelson interferometers made this type of devices suitable only for laboratory conditions. In 2003, Hast [10] proposed a new self-mixing interferometry method that enabled simple, compact, and cheap interferometer devices to be implemented. No direct contact between the laser device and the skin is required, but still the sensor needs to operate in close proximity to the subject. The main drawback of this type of sensing is noise introduced by skin displacement due to motion and involuntary muscular contraction.

All the aforementioned methods use either contact or close-proximity sensing and require the subject's cooperation. In psycho-physiological experiments, it is important to measure physiological responses without interfering at all with the subject, or a variable may be introduced to his psychological state [11]. In these cases, a contact-free measurement methodology for measuring vital signs (e.g., pulse) at a comfortable distance is very appealing. The first contact-free vital sign measurement method based on active sensing was introduced by Greneker in 1997 [12]. The radar vital signs monitor (RVSM), as it is called, it is able to measure the subject's heartbeat and respiration rate at a distance up to 30 feet without the requirement of a physical connection to the subject. The RVSM antenna is bore sighted on the thorax region of the subject's chest. It detects

Manuscript received February 21, 2006; revised November 29, 2006. This work was supported in part by the National Science Foundation (NSF) under Grant IIS-0414754. Any opinions, findings, and conclusions or recommendations expressed in this material are those of the authors and do not necessarily reflect the views of the funding agency.

M. Garbey and N. Sun are with the Department of Computer Science, University of Houston, Houston, TX 77204-0101 USA.

*I. Pavlidis is with the Department of Computer Science, University of Houston, Houston, TX 77204-0101 USA (e-mail: ipavlidi@central.uh.edu).

A. Merla is with the Department of Clinical Sciences and Bioimaging, Fondazione Università Gabriele d'Annunzio - Chieti, 66100 Chieti, Italy.

Digital Object Identifier 10.1109/TBME.2007.891930

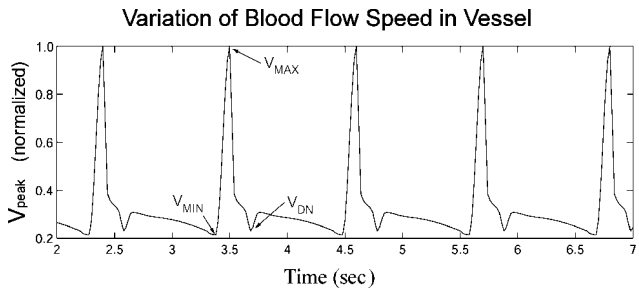

Fig. 1. Pulse waveform given by Doppler ultrasound [4].

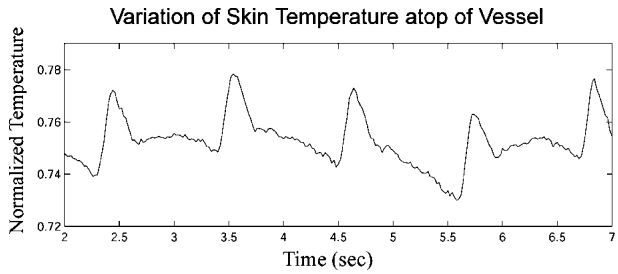

Fig. 2. Pulse waveform given in temperature modulation format produced by the 2-D unsteady bioheat model [14].

the shock wave initiated from the beating heart while it spreads across the thorax region of the chest wall. The measurement may be contaminated by body motion, which presents a much larger Doppler modulated radar cross-section than the small heartbeat-induced movement of the chest wall.

To the best of our knowledge, no contact-free pulse measurement method based on passive sensing has been demonstrated so far. Recently, Pavlidis *et al.* have proposed a series of bioheat and statistical models that in combination with customized highly sensitive TI hardware can measure various physiological variables at several feet away from the subjects. These include contact-free measurements of perfusion [13], vessel blood flow [14], and breathing rate [15]. Since all these methods are based on passive imaging are absolutely safe and suitable for long observation periods.

In CVPR 2005, the authors proposed for the first time an FFT-based computational method to measure cardiac pulse via TI of a major superficial vessel [16]. In this paper, we elaborate further on that method and we present new experimental results and operational analysis. Specifically, we present a brief introduction to the pulse physiology in Section II. In Section III, we describe how to select and track the line-shaped region of interest on the tissue imagery. In Section IV, we describe a novel method to apply FFT along this line-shaped region to capitalize upon the pulse's thermal propagation effect. In Section V, we describe the estimation function we apply on the average FFT result to extract the heartbeat frequency. In Sections VI and VII, we discuss the experimental setup and the method's performance respectively. We conclude the paper in Section VIII.

II. Cardiovascular Pulse

The cardiovascular pulse is generated in the heart, when the left ventricle pumps blood to the body. The blood travels through the arterial network and returns back to the heart through the vein network. Different mechanical processes are involved into the propagation of the cardiac pulse. Therefore, the pulse waveform can be described in terms of blood velocity, blood flow rate, and blood pressure. A comprehensive annotation to the pulse waveform was presented by Holdsworth in 1999 [4]. In that research, measurements were carried out on the carotid of the subjects by using Doppler ultrasound. Seven feature points correlated to the vascular fluid dynamics were identified as waveform descriptors (see Fig. 1). Comparing 3560 carotid waveforms from 17 subjects, the study reported negligible contralateral differences. This indicated that pulse waveforms of normal subjects have similar shapes.

In this paper, we are interested in monitoring cardiovascular pulse through analysis of skin temperature modulation. Pulsative blood flow modulates tissue temperature because of the heat exchange by convection and conduction between vessels and surrounding tissue. Such modulation is more pronounced in the vicinity of major superficial blood vessels.

In [14], we have proposed a model to simulate the heat diffusion process on the skin initiated by the core tissue and a major superficial blood vessel. We also took into account noise effects due to the environment and instability in the blood flow. Our simulation demonstrated that the skin temperature waveform is directly analogous to the pulse waveform. But, its exact shape is smoothed, shifted, and noisy with respect to the originating pulse waveform due to the diffusion process. Fig. 2 shows the skin temperature modulation computed by the 2-D unsteady bioheat model in [14]. Comparing Fig. 1 with Fig. 2, we observe that some feature points which provide fine detail are missing, but the basic periodicity is present in both waveforms. This indicates that the pulse can be recovered from the skin temperature modulation recorded with a highly sensitivity thermal camera and processed through an appropriate signal analysis method.

Fig. 3(a) shows a characteristic temperature profile collected from a small portion of the carotid region of a subject shown in Fig. 3(c). The signal has been affected by systemic noise and air circulation on the skin. Because our experiments are set up in a quite indoor environment and we test healthy subjects who are relaxed during the recording, it is reasonable to assume that their pulse should range between 40 and 100 beats per minute (bmp). Therefore, we can facilitate pulse recovery by removing signals with frequency lower than 0.67 Hz (40 bmp) and higher than 1.67 Hz (100 bmp). Fig. 3(b) shows the result after removing the noise. Even though the amplitude of the waveform is unstable, periodicity is evident and the signal is very similar to Fig. 2, which is the simulated result of our bioheat model. This further corroborates our hypothesis that the pulse can be recovered from the dynamic temperature profile of skin.

III. Regions of Interest

As a consequence of the tissue thermal diffusion, modulation of skin temperature is strongest along the superficial blood vessels. This is also predicted by our bioheat transfer model reported in [14] and has been verified by our experiments. Based on clinical and anatomical knowledge [17], [18], we extract the cardiac pulse from major superficial vessels on the face, a tissue area that is usually exposed naked. Typically, we focus either on the external carotid [Fig. 4(a)] or the superficial temporal

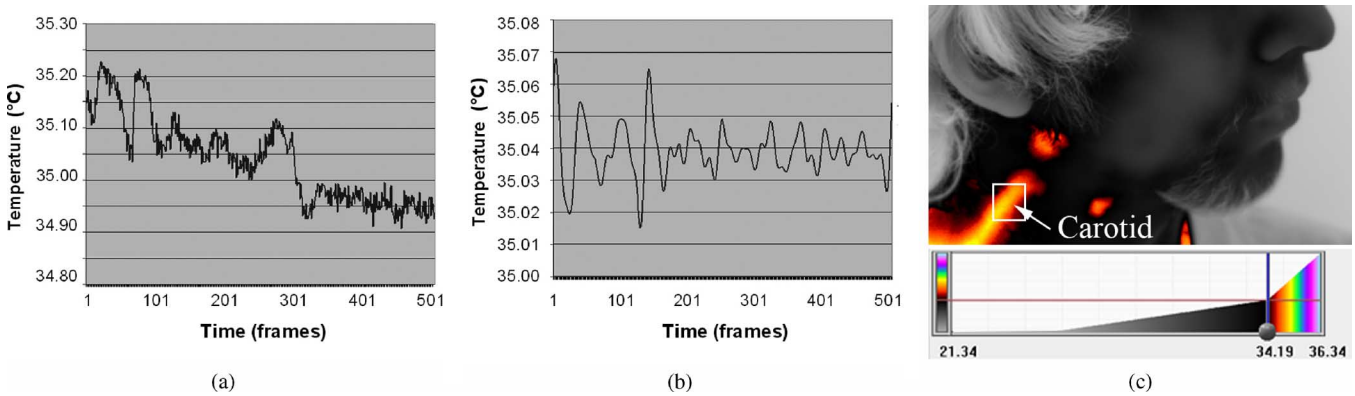

Fig. 3. (a) Raw temperature profile along the timeline. (b) Temperature profile after removing frequency signals lower than 0.67 Hz (40 bmp) and higher than 1.67 Hz (100 bmp). (c) Collection point on the carotid artero-venous complex of the subject.

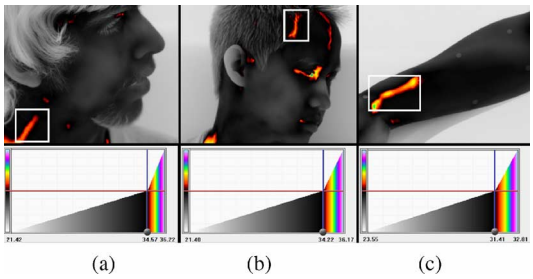

Fig. 4. Pulse taking locations: (a) Carotid vessel complex. (b) Superficial temporal vessel complex. (c) Radial vessel complex.

artero-venous complex [Fig. 4(b)]. It is also possible to extract the pulse from other parts of the body where major superficial vessels exists. An example is the case of the radial artero-venous complex [Fig. 4(c)] in the wrist.

Presently, we select the skin footprint of the vessel complex by manually drawing a line on the imagery through the graphical user interface. Therefore, the outcome depends on the skill and knowledge of the operator. In the future, vessel localization can be performed automatically by the computer, based on a superficial blood vessel segmentation method proposed by Buddharaju *et al.* [19].

IV. Pulse Measurement Methodology

Our method is based on the assumption that temperature modulation due to pulsating blood flow produces the strongest thermal signal on a superficial vessel. This signal is affected by physiological and environmental thermal phenomena. Therefore, the resulting thermal signal that is being sensed by the thermal camera is a composite signal, with the pulse being only one of its components. Our effort is directed into recovering the frequency of the component signal with the highest energy content. This is consistent with our hypothesis of pulse dominance in the thermal field of a superficial vessel.

As we mentioned in Section III, we select interactively the pulse taking location in the first frame of the thermal video. A prerequisite to accurate pulse measurement is motion tracking. Even when subjects are instructed to stay put, they still exhibit slight movements due to motor functions. We use a conditional density propagation tracker [20] with thresholding as its feedback mechanism. The tracker allows meaningful application of Fourier analysis on the vessel's region of interest in the presence of tissue motion. Based on the outcome of Fourier analysis an estimation function computes the cardiac pulse. Fig. 5 illustrates the general steps of our methodology.

Considering that the blood vessel is a long, narrow structure, the pulse propagation phenomenon causes slight phase shift on the temperature profiles along the blood vessel. This may weaken the signal if we use conventional signal recovery methods in the time domain. Each pixel along the blood vessel has a unique periodical temperature profile, which is shifted with respect to the others. As Fig. 6 shows, averaging these temperature profiles may weaken the signal. Although, the temperature profiles of the pixels along the blood vessel are shifted in the time domain, their frequency should remain the same (unshifted). Therefore, by operating on the frequency domain and combining appropriately the power spectra of these temperature profiles we can reinforce the signal instead of weakening it. We apply Fourier analysis in a novel manner to capitalize upon the pulse propagation effect and extract the dominant pulse frequency:

A. First Step

We select a straight segment L along the center line of a large superficial blood vessel. The algorithm expands symmetrically L into an elongated rectangle R. The width of this rectangle depends on the width of the vessel on the thermal imagery. For a subject imaged at 6 feet with a 50-mm lens the rectangle's width is 3–7 pixels. By convention, we place the x axis of our coordinate system along the width and the y axis along the length of the vessel (see Fig. 7).

B. Second Step

We record the time evolution of the pixel matrix delineated by rectangle R for N frames ($N = 256$ or 512). Thus, we produce a 3-D matrix $A(x, y, t)$, where $0 \leq x \leq R_x$, $0 \leq y \leq R_y$ is the spatial extent of rectangle R and $0 \leq t \leq N-1$ is the timeline.

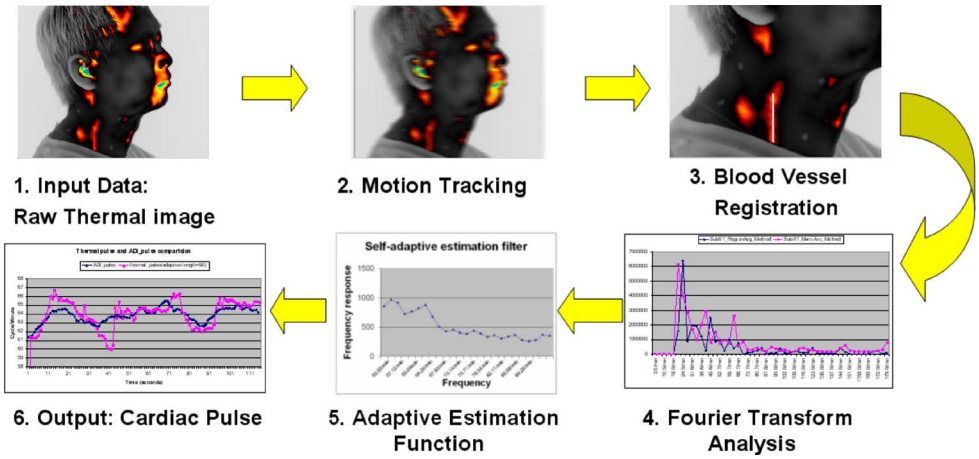

Fig. 5. Pulse measurement methodology.

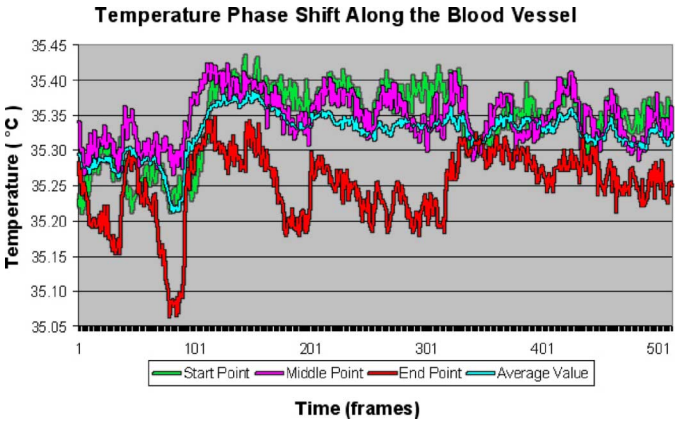

Fig. 6. Temperature profiles of three different pixels along the exposed blood vessel of a subject compared to the average temperature profile.

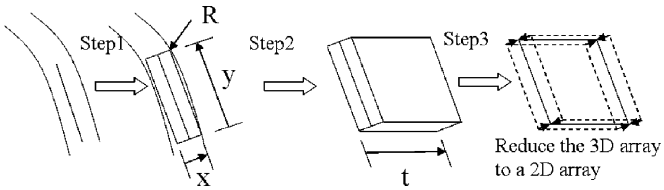

Fig. 7. Schematic diagram of the first three steps in our Fourier analysis of the vessel temperature signal.

C. Third Step

We average the pixel temperatures along the x dimension. Thus, we derive a 2-D matrix

$$A'(y,t) = \frac{1}{R_x}\sum_{x=0}^{R_x} A(x,y,t) \tag{1}$$

where $0 \le y \le R_y, 0 \le t \le N-1$. This reduces the noise and "shrinks" the rectangular vessel region R into an *effective* line, upon which the signal measurement will be performed.

D. Fourth Step

For each *effective* pixel on the measurement line we obtain the time evolution signal of its temperature [see Fig. 8(a)]

$$\{\forall y : S_y(t) = A'(y,t), 0 \le t \le N-1\}. \tag{2}$$

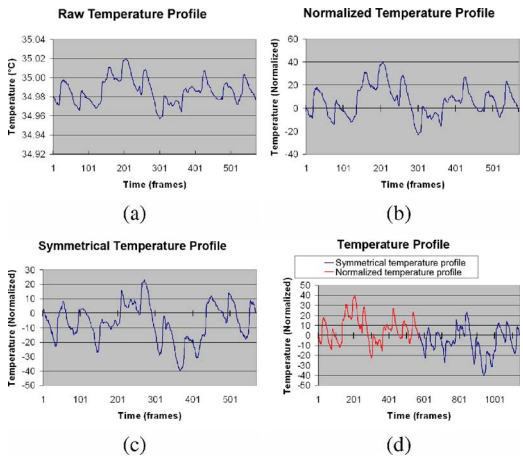

Fig. 8. (a) Raw temperature profile of an effective vessel pixel. (b) Normalized temperature profile. (c) Symmetrical temperature profile. (d) Periodic extension (normalized followed by symmetrical).

We apply the fast Fourier transform (FFT) on each of these signals (temperature profiles) to obtain the respective power spectra

$$\{\forall y : P_y = F(S_y(t))\}. \tag{3}$$

The FFT method was first introduced by Cooley and Tukey (1965) [21]. Thereafter, it was used widely in signal analysis due to its high efficiency in comparison to other methods, such as the solution of linear equations or the correlation method [22]. To apply the FFT on the temperature profile of each effective pixel, first we use a low-order trigonometric polynomial as follows:

$$U_y(t) = S_t - (\alpha\cos(t) + \beta) \tag{4}$$

with $\alpha = (1/2)(S_y(0) - S_y(N-1))$, $\beta = (1/2)(S_y(0) + S_y(N-1))$. This ensures that the shift will not affect the stability of the scheme by minimizing the Gibbs phenomenon. The output is a normalized profile as shown in Fig. 8(b). Then, we

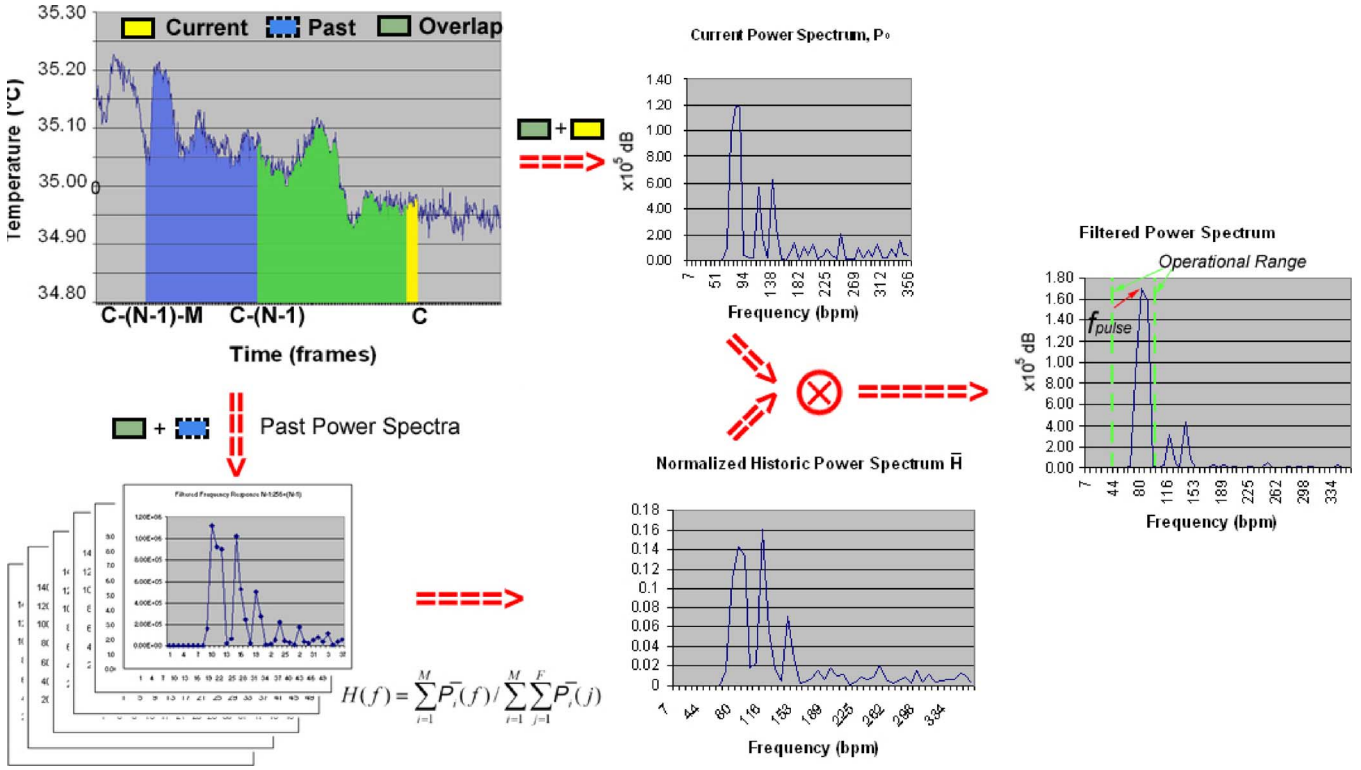

Fig. 9. Pulse estimation process based on current and past data. The operational frequency band is delineated in green and corresponds to the pulse range that is relevant to the experimental scenario. The power content of frequencies outside the operational range is excluded from consideration. In our experiment, the operational range was set to [40,100] bpm, which corresponds to the baseline physiology of healthy subjects. This range may expand in case pathological or physically strained subjects are involved.

construct out of this normalized profile a periodic function by first applying the symmetry [see Fig. 8(c)]

$$\forall t \in (0, N), U_y(N - t) = -U_y(t) \tag{5}$$

and then the periodic extension [see Fig. 8(d)]

$$\forall t \in (0, 2N), \forall k \in Z, U_y(t + k2N) = U_y(t). \tag{6}$$

We apply a classical decimation-in-time (Cooley and Tukey) 1-D base-2 FFT method given in [23].

E. Fifth Step

We average all the power spectra computed in the previous step into a composite power spectrum

$$\bar{P} = \frac{1}{R_y} \sum_{y=0}^{R_y} P_y. \tag{7}$$

V. Adaptive Estimation Function

A fundamental question is what we report as the effective pulse along the timeline. The instantaneous computation described in Section IV is not to be trusted literally since it may be affected occasionally by thermoregulatory vasodilation and creeping noise. To address this problem we use an estimation function that takes into account the current measurement as well as a series of past measurements. Our estimation function is similar to adaptive line enhancement [24].

The current power spectrum $\bar{P}_0$ of the temperature signal is being computed over the previous N frames ($N = 256$ or 512) by applying the process outlined in the previous section. We convolve the current power spectrum with a weighted average of the power spectra computed during the previous M time steps (see Fig. 9). We chose $M = 60$, since at the average speed of 30 fps sustained by our system, there is at least one full pulse cycle contained within 60 frames even in extreme physiological scenarios. Therefore, the historical contribution to our estimation function remains meaningful at all times.

Specifically, the historical frequency response at a particular frequency f is given as the summation of all the corresponding frequency responses for the M spectra, normalized over the total sum of all the frequency responses for all the historical M spectra

$$H(f) = \frac{\sum_{i=1}^{M} \bar{P}_i(f)}{\sum_{i=1}^{M} \sum_{j=1}^{F} \bar{P}_i(j)}. \tag{8}$$

Finally, we convolve the historical power spectrum $\bar{H}$ with the current power spectrum to filter out transient features. We then designate as pulse the frequency f_{pulse} that corresponds to the highest energy value of the filtered spectrum within the operational frequency band (see Fig. 9).

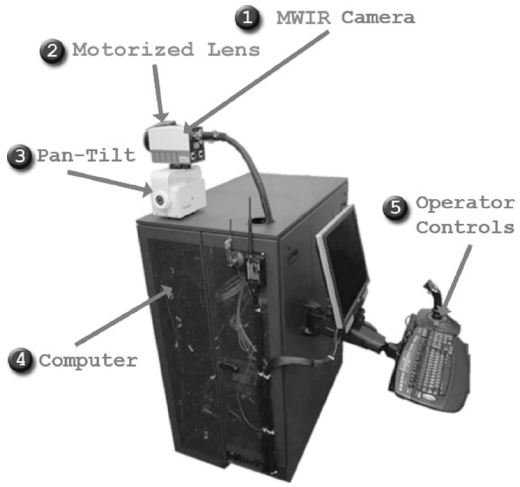

Fig. 10. TI system.

VI. Experimental Setup and Design

We have used a high-quality TI system for data collection. We have designed the architecture of the TI system with one primary goal in mind: measurement accuracy. The system is composed of several off-the-self components that have been custom retrofitted to support the task at hand (see Fig. 10). The centerpiece of the system is a MWIR camera [25]. It features an Indium Antimonide (InSb) high efficiency photon detector that yields temperature resolution < 25 mK. The camera is capable of capturing 30 fps in full spatial resolution (640×480 pixels). The electronic shutter speed ranges from 9 μs to the full frame speed.

The camera is fitted with a MWIR 50-mm lens. This lens allows focusing on parts of the subject with rich superficial vasculature (e.g., face) at distances between 3 and 10 feet. These distances are typical in psycho-physiological laboratory experiments.

The camera sits atop a pan-tilt device to allow flexible positioning. We also use a differential blackbody as a calibrating device. The blackbody's temperature resolution matches that of the thermal camera's.

All the aforementioned hardware components communicate with a powerful workstation and are placed in a cart for maximum portability (see Fig. 10).

The TI measurements are compared against a "ground-truth standard." The GT standard is provided through the measurements of a high-quality contact sensing device. This device is composed of the following items:

1) a ML750 PowerLab/4SP data acquisition system from ADInstruments [3];
2) a ML116 GSR Amp from ADInstruments [3];
3) two MLT 1010 piezoelectric pulse transducers from ADInstruments [3].

During the experiment the subject sits about 6 feet away from the TI system. A MLT 1010 piezoelectric pulse transducer is wired to the subject's index finger tip (see Fig. 11). The subject is briefed and after that she/he signs the consent document. Subjects suffering from neuropathies, micro or macro-angiopathy, as well as strong smokers have been excluded from this study.

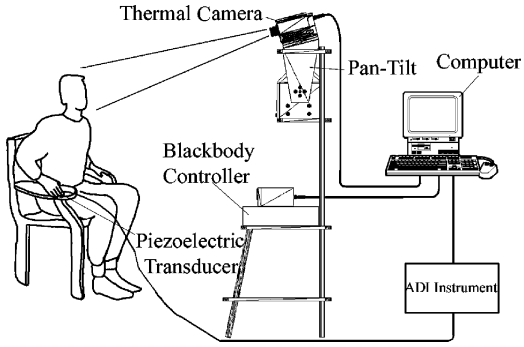

Fig. 11. Experimental setup.

For each subject, we record up to 5 min of thermal video in a restful state. We image primarily the subject's face because it is conveniently exposed and features multiple locations with large superficial vessels (e.g., carotid and temporal areas).

VII. Experimental Results

We have recorded 34 thermal clips from 34 subjects while resting in an armchair. Concomitantly we have recorded GT pulse signals with the ML750 PowerLab/4SP data acquisition system. The sample features subjects of both genders, different ages, and with varying physical characteristics. Measurement for each subject was performed in a single session.

Because our TI system and the ML750 PowerLab/4SP data acquisition system have different frequency of sampling and perform measurements on a vastly different theoretical basis, we need first to normalize the experimental data from the two modalities in order to compare them.

The ML 750 PowerLab/4SP data acquisition system (GT) collects 100 samples/second, while our TI system acquires 30 frames/second (fps). We average the ground truth output data every 10 samples while the infrared TI data every three samples (frames). Based on this normalization, we have compared the average cardiovascular pulse rate computed by our imaging method to that reported by the GT instrument for all the subjects in our data set. The comparison is based on the complement of the absolute normalized difference (CAND)

$$\mathrm{CAND} = 1 - \frac{|\mathrm{GT} - \mathrm{TI}|}{\mathrm{GT}} \tag{9}$$

which is the absolute difference between the TI and GT measurements normalized against the GT and subtracted from unity. This gives a weighted indication of how close the TI measurement is to the GT measurement in each case.

Table I shows the detailed profile of our comparative experiment and the average pulse measurements reported by the two modalities. The overall CAND of the mean pulse computation versus the GT is 88.52%. The performance improves to 90.33% when only 21 subjects with relatively clearer vessel thermal imprint are considered. These are typically leaner subjects where the vessel of interest is not under a thick layer of fat (see Fig. 12). A major difference between this experiment and the one we reported in CVPR 2005 [16] is that this time the subjects were given more freedom to move during the recording.

TABLE I
COMPARISON OF GT AND TI PULSE MEASUREMENTS.

Subject Code	Gender	Tissue	Thermal Imprint	GT Pulse (bmp)	TI Pulse (bmp)	$CAND$ %
Subject 01	Male	Carotid	Clear	75.9	63.8	84.02
Subject 03	Male	Carotid	Clear	68.8	63.7	92.62
Subject 04	Male	Carotid	Not Clear	63.3	60.5	95.60
Subject 06	Male	Temporal	Not Clear	59.9	67.3	87.65
Subject 07	Male	Carotid	Clear	68.0	61.4	90.32
Subject 08	Male	Temporal	Clear	72.5	63.6	84.21
Subject 09	Male	Carotid	Clear	72.6	67.9	93.53
Subject 10	Male	Carotid	Clear	82.3	66.9	81.25
Subject 11	Male	Carotid	Clear	83.3	76.8	92.17
Subject 12	Male	Carotid	Not Clear	63.8	62.8	98.43
Subject 13	Male	Carotid	Clear	64.7	64.4	99.58
Subject 15	Male	Carotid	Clear	76.9	62.3	80.99
Subject 16	Male	Carotid	Not Clear	57.2	63.2	89.54
Subject 17	Female	Carotid	Clear	67.4	63.6	94.32
Subject 19	Female	Carotid	Clear	70.5	62.3	88.34
Subject 20	Female	Carotid	Not Clear	81.1	57.4	70.72
Subject 21	Male	Carotid	Clear	75.2	72.2	96.00
Subject 22	Female	Supra-Orbital	Clear	77.1	74.3	96.32
Subject 23	Male	Carotid	Not Clear	76.1	67.8	89.09
Subject 24	Male	Carotid	Not Clear	55.6	78.1	59.63
Subject 25	Male	Carotid	Not Clear	61.6	74.1	79.77
Subject 26	Female	Carotid	Not Clear	62.9	61.1	97.19
Subject 27	Female	Temporal	Not Clear	62.4	62.9	99.17
Subject 28	Female	Carotid	Clear	74.0	73.1	98.81
Subject 29	Male	Temporal	Clear	74.6	65.4	87.65
Subject 31	Female	Carotid	Clear	70.7	58.1	82.22
Subject 33	Male	Carotid	Not Clear	86.1	65.4	75.91
Subject 34	Male	Carotid	Not Clear	79.3	61.1	77.06
Subject 35	Male	Carotid	Not Clear	59.9	64.1	92.95
Subject 36	Female	Carotid	Clear	68.3	72.9	93.28
Subject 37	Male	Carotid	Clear	67.5	60.9	90.15
Subject 38	Male	Temporal	Clear	75.1	63.3	84.24
Subject 39	Female	Carotid	Clear	72.3	71.8	99.31
Subject 40	Male	Supra-Orbital	Clear	70.6	61.9	87.71

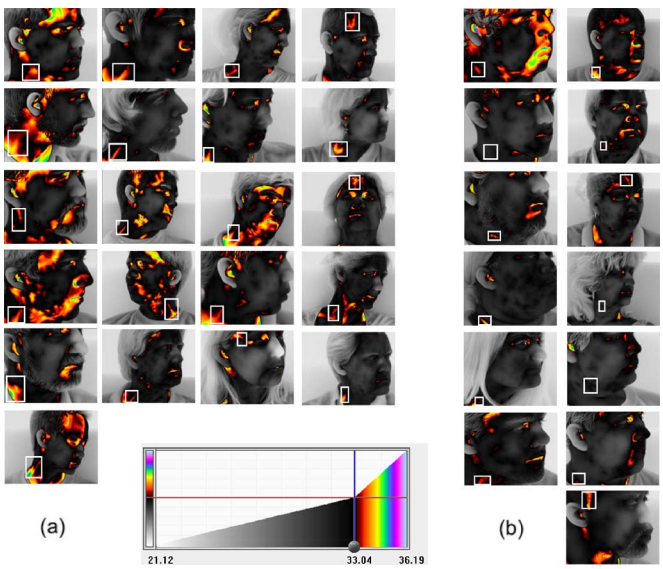

Fig. 12. Thermal snapshots of all 34 subjects. (a) Subjects with relatively clear vessel thermal imprint. (b) Subjects with relatively unclear vessel thermal imprint.

The recording itself was also longer (5 min versus 2 min). Although, the tracker coped well with most of the motion, obviously it is far from perfect. The noise introduced due to tracking imperfections causes damage to the performance of the method that is comparable (if not larger) than that of an unclear vessel imprint.

Another issue is how the method will fare in difficult environmental or physiological conditions (e.g., strong air currents or high heat or high fever). This was not addressed in this study, but we expect that environmental perturbations will seriously affect the performance of the method, only if they are in the same frequency range as pulsation (e.g., periodic air currents) or result in excessive perspiration (e.g., prolonged high heat or high fever) that alters non-linearly the thermal map of the skin.

In normal indoor conditions, such as those we studied, the thermal pulsation signal that travels along the length of the vessel is harvestable but weak. The current experimental results demonstrate that passive measurement of pulse at a distance is absolutely feasible, but its performance can be further improved only through more sophisticated methods of noise reduction and motion cancelation.

VIII. CONCLUSION AND FUTURE WORK

We presented a novel measurement method of cardiovascular pulse. The method is based on TI and exploits the periodic properties of the cardiac pulse's thermal field through Fourier signal analysis. An adaptive estimation function ensures robust selection of the pulse frequency in the presence of signal noise. Since the method is contact-free, passive, and highly automated

(imaging tracker), it opens the way for sustained physiological measurements in the most transparent manner.

Almost all the conventional methods require contact and hence they compromise the subject's comfort to one degree or another. This is especially important in psychophysiology where intrusive sensing is undesirable. The contact-free pulse measurement method reported here adds to the set of other contact-free measurement methods reported earlier for different vital signs (i.e., breath and superficial perfusion). Therefore, it is part of a growing set of vital sign measurements at a distance, under a single sensing regime (TI).

Our method exhibits good accuracy when compared to piezoelectric pulse measurements, which is used in standard clinical practice. The experimental results clearly demonstrate the feasibility of the approach. A conditional density propagation tracker coped well with small head motion, although more sophisticated tracking is needed to improve the performance further. Overall, we feel that there is amble room for further performance improvements through better noise reduction methodologies. This is one of the areas our ongoing research is focused on.

Our current method can only retrieve the cardiovascular pulse rate. We are in the process of merging this method with the inverse problem solution we developed in [14] to recover the amplitude of the pulse waveform. The extraction of the full pulse waveform may open broader biomedical applications.

ACKNOWLEDGMENT

Research activity involving human subjects has been reviewed and approved by the University of Houston Committee for the Protection of Human Subjects. The authors would like to thank all the volunteer subjects who participated in their test population. They would also like to thank Dr. E. Glinert from the National Science Foundation (NSF) for his support and encouragement in this nascent technology effort. Equally, they would like to thank Dr. J. Levine from the Mayo Graduate School of Medicine for his valuable feedback.

REFERENCES

[1] A. C. Guyton, *Textbook of Medical Physiology*, 8th ed. Philadelphia, PA: Saunders, 1991, ch. 11.

[2] K. Aminian, X. Thouvenin, P. Robert, J. Seydoux, and L. Girardier, "A piezoelectric belt for cardiac pulse and respiration measurements on small mammals," in *Proc. 14th Annu. Int. Conf. IEEE Engineering in Medicine and Biology Society*, 1992, pp. 2663–2664.

[3] PowerLab ADInstruments Owner's Manual. Castle Hill, NSW, Australia, ADInstruments Pty Ltd., 2004.

[4] D. W. Holdsworth, "Characterization of blood-flow waveforms in normal human subjects," *Physiol. Meas.*, vol. 20, no. 3, pp. 219–240, Aug. 1999.

[5] J. Allen and A. Murray, "Similarity in bilateral photoplethysmographic peripheral pulse wave characteristics at the ears, thumbs and toes," *Physiol. Meas.*, vol. 21, pp. 369–377, Aug. 2000.

[6] P. J. Chowienczyk, "Photoplethysmography assessment of pulse wave reflection: Blunted response to endothelium-dependent beta2-adrenergic vasodilation in type ii diabeters mellitus," *J. Am. Coll. Cardiol.*, vol. 34, no. 7, pp. 2007–2014, Dec. 1999.

[7] T. Wu, "PPGI: New development in noninvasive and contactless diagonosis of dermal perfusion using near infrared light," *J. Soc. Chinese Physists Germany*, vol. 7, no. 1, pp. 17–24, Oct. 2003.

[8] J. Allen and A. Murray, "Photoplethysmography – A tool for assessing the microcirculation," in *Thermol. Int.*, 2002, vol. 12, pp. 69–70.

[9] S. S. Ul'yanov and V. V. Tuchin, "Pulse-wave monitoring by means of focused laser beams scattered by skin surface and membranes," *Proc. SPIE*, vol. 1884, pp. 160–167, 1993.

[10] J. Hast, "Self-mixing interferometry and its applications in non-invasive pulse detection," Ph.D. dissertation, Oulu Univ., Dept. Electr. Inf. Eng., , Finland, 2003.

[11] I. Pavlidis, N. L. Eberhardt, and J. Levine, "Human behavior: Seeing through the face of deception," *Nature*, vol. 415, no. 6867, p. 35, Jan. 2002.

[12] E. F. Greneker, "Radar sensing of heartbeat and respiration at a distance with application of the technology," *RADAR*, vol. 97, no. 449, pp. 150–154, Oct. 1997.

[13] I. Pavlidis and J. Levine, "Monitoring of periorbital blood flow rate through thermal image analysis and its application to polygraph testing," in *Proc. 23rd Annu. Int. Conf. IEEE Engineering in Medicine and Biology*, Istanbul, Turkey, Oct. 25–28, 2001, vol. 3, pp. 2826–2829.

[14] M. Garbey, A. Merla, and I. Pavlidis, "Estimation of blood flow speed and vessel location from thermal video," in *Proc. 2004 IEEE Computer Society Conf. Computer Vision and Pattern Recognition*, Washington, D.C., Jul. 2, 2004, vol. 1, pp. 356–363.

[15] R. Murthy, I. Pavlidis, and P. Tsiamyrtzis, "Touchless monitoring of breathing function," in *Proc. 26th Annu. Int. Conf. IEEE Engineering in Medicine and Biology*, San Francisco, CA, Sep. 1–5, 2004, vol. 2, pp. 1196–9.

[16] N. Sun, M. Garbey, A. Merla, and I. Pavlidis, "Imaging the cardiovascular pulse," in *IEEE Comput. Soc. Conf. Computer Vision and Pattern Recognition*, San Diego, CA, Jun. 20–25, 2005, pp. 416–421.

[17] F. H. Martini, *Fundamentals of Anatomy & Physiology*, 6th ed. San Francisco, CA: Benjamin Cummings, 2004, p. 753.

[18] R. R. Seeley, T. D. Stephens, and P. Tate, *Anatomy & Physiology*, 6th ed. New York: McGraw Hill, 2003, p. 746.

[19] P. Buddharaju, I. T. Pavlidis, and P. Tsiamyrtzis, "Physiology-based face recognition," in *Proc. IEEE Int. Conf. Advanced Video and Signal Based Surveillance*, Como, Italy, Sep. 15–16, 2005, pp. 354–359.

[20] M. Isard and A. Blake, "Condensation – Conditional density propagation for visual tracking," *Int. J. Comput. Vis.*, vol. 19, no. 1, pp. 5–28, 1998.

[21] J. W. Cooley and J. W. Tukey, "An algorithm for the machine calculation of complex Fourier series," *Math. Computation*, vol. 19, pp. 297–301, 1965.

[22] S. W. Smith, *The Scientist and Engineer's Guide to Digital Signal Processing*, 2nd ed. San Diego, CA: California Tech. Pub., 1999, ch. 12, pp. 225–42.

[23] W. H. Press, S. A. Teukolsky, W. T. Vetterling, and B. P. Flannery, *Numerical Recipes in C*, 2nd ed. New York: Cambridge Univ. Press, 1992, ch. 12, pp. 504–21.

[24] M. Akay, Y. M. Akay, W. Welkowitz, J. L. Semmlow, and J. B. Kostis, "Application of adaptive filters to noninvasive acoustical detection of coronary occlusions before and after angioplasty," *IEEE Trans. Biomed. Eng.*, vol. 39, no. 2, pp. 176–184, Feb. 1992.

[25] Indigo Systems Inc., Goleta, California [Online]. Available: http://www.indigosystems.com

Marc Garbey received the Ph.D. degree from the Ecole Centrale de Lyon, Lyon, France, in 1984 and his Habilitation from University of Lyon in 1989.

He is a Professor of Applied Mathematics and Computer Science at the University of Houston, Houston, TX. He is also the Chair of the Computer Science Department at the same university. His research focuses on modeling of physiological systems using partial differential equations.

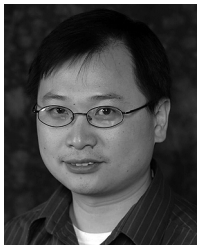

Nanfei Sun received the B.A. degree (with honors) from the Chongqing Jianzhu University, Chongqing, China, in 1994, the M.S. degree in computer science from the University of North Carolina at Charlotte in 2001, and the Ph.D. degree in computer science from the University of Houston, Houston, TX, in 2006.

While at the University of Houston, his research was supported by the National Science Foundation. His research interests include thermal imaging, computer vision, pattern recognition, and digital signal processing.

Arcangelo Merla holds a Ph.D. in advanced biomedical technologies and bioimaging from the University of Chieti (Italy) and a M.S. (laurea) in physics from the University of Bologna (Italy). His expertise is in the area of biomedical imaging and modeling, with special emphasis on infrared imaging and its biomedical applications. Dr. Merla published extensively in these areas in biomedical journals and refereed conference proceedings over the past years. Dr. Merla had joined the faculty of the Clinical Sciences and Bioimaging Department – School of Medicine, at the University of Chieti as of August 2002. He is the Director of the Functional Infrared Imaging Lab at ITAB – Institute of Advanced Biomedical Technologies of the University G. D'Annunzio in Chieti-Pescara and Visiting Assistant Professor at the Computational Physiology Lab of the University of Houston.

Ioannis Pavlidis is the Eckhard Pfeiffer Professor of Computer Science and Director of the Computational Physiology Lab at the University of Houston, Houston, TX. His research is funded by multiple federal agencies including the NSF, DOD, DHS, and NIH and corporate sources. He has written many journal articles and books on the topics of computational physiology, computational psychology, computer vision, and pattern recognition. He is famous for his work on stress quantification, which appeared in *Nature* and the *Lancet*, and received world-wide scientific and media attention. He has also established several well-known IEEE Conferences and Workshops, among them the IEEE Advanced Video and Signal Based Surveillance (AVSS) Conference. He also served and continues to serve in many advisory panels to DARPA and other federal agencies. He is a Fulbright fellow.